University of Reading
Department of Mathematics and Statistics

Declaration

I con rm that this is my own work and the use of all material fro m other sources has been properly and fully acknowledged.

Publications Ar

Edg1790 275260 ngton, M. ad

List of Figures

. t44351(3938ET 26a.6988(.)-500.985(.)-500.161(.)-500.985(.)-500.985(.)-500.985(.)-500.161(.)-500.985(.)-1159.34

List of Tables

Chapter 1

Introduction

The aim of this thesis is to formulate and analyse mathematical models of intracellular signalling pathways describing chemotactic cell movement in *Escherichia coli* and *Rhodobacter sphaeroides* cells. In particular, this allows us to link single cell behaviour to the population scale by using well informed and analysed single cell models. We also seek to utilise knowledge gained from *E. coli* studies to inform models of the more complex bacterial species *R. sphaeroides*.

In order to make sense of the term chemotaxis we may break it down into the prefix 'chemo'

Chapter 3 is able to display an overshoot response to ligand stimuli. In doing so a number of key processes in the signalling cascade are identified as responsible for the emergence of the response. Results are compared with experimental data and discussed with reference to their biological feasibility.

An agent-based model (ABM) is developed in Chapter 6 to understand how individual behaviour identified in Chapters 3 to 5 maps to the population scale. Using this ABM we further these single cell investigations by studying phenomena in the context of chemotactic *E. coli* cell populations. In particular, the effects of variation in intracellular signalling protein concentra-

postulating a new *R. sphaeroides* signalling model and show that this helps to remove some of the issues associated with previous modelling efforts.

Finally, in Chapter 9 a summary of the work contained within this thesis shall be given. Within the context of this summary, the implications of this work both for the future study of chemotaxis signalling pathways as well as other biological systems will be discussed.

In addition to the work discussed in Chapters 1-9, Appendices A-E provide further details on mathematical results and biological concepts referred to within this thesis for the interested reader. To this end a glossary of important biological terms appearing within this thesis is also included.

2.2 Mathematical Modelling of the Single Cell

From the early 1970s onward there has been a large amount of theoretical work aimed at understanding bacterial chemotaxis. The majority of this w

where

and j -th receptors, respectively, J_{ij} denotes the coupling strength between receptors and $B_i(t)$ is the attractant concentration. When no attractant bindin g occurs, each receptor may freely switch between their two states.

The rst application of this type of model to chemoreceptor coupling was due to Shi & Duke [51]. Using mean- eld theory they demonstrated that the coupling strength of neighbouring receptors had a large e ect upon the sensitivity of a recptor array, however adaptation was not studied in great detail within this work. Duke & Bray [52] later conducted Monte Carlo simulations of this model in which each receptor was coupled to its four closest neighbours. These simulations were able to show that changes in attracta

of the experimental data, their main weakness is in their com

the incorporation of an MWC description of receptor clustering. In this work they discuss the existence of cell-to-cell variation in methylation and demethylation rates which is proposed to be a survival/bet hedging strategy allowing for population survival in varied environments. In addition they note the ability of their model to display the experimentally observed asymmetry in adaptation time for addition or removal of attractant.

The experiments of Li & Hazelbauer [67] were the focus of work by Endres & Wingreen [68]. Li & Hazelbauer [67] observed that the adaptation proteins CheB and CheR can bind an approximately 35 amino acid tether allowing them to act upon groups of between five and seven receptors, termed an \assistance neighbourhood". The work of Endres & Wingreen [68] then sought to examine this effect by incorporating an adaptation model, similar to Barkai & Leibler [44], into an MWC one. In doing so they found two different responses for high attractant concentrations. In particular, it was noted that the response could either be terminated by receptor saturation (i.e. no further ligand binding is possible) or for large stimuli, receptors may become fully methylated. At this point, low affinity binding of aspartate to Tsr receptors can allow the cell to respond to further stimuli. Hansen et al. [69] extended this by explicitly considering the actions of CheR and CheB in the form of an ODE for the average methylation level of receptors within a cluster.

More recently, Clausznitzer et al. [70] considered an MWC modelling approach combining much of the MWC modelling work discussed above. Within this work the kinetics of the average receptor methylation level (

It is clear from the work summarised here that MWC models are able to produce good agreement with the experimental literature in terms of receptor sensitivity and gain. In particular,

Firstly, some cells will move outward using up serine until they reach the outer ring of the serine. Then, of those which remain, some will move outward in search of aspartate, forming a second ring. Finally, some of the remaining cells will search for threonine, forming a third ring. The observation of these chemotactic bands was a key factor in sparking an interest in the modelling of population scale behaviour.

2.3.1 Keller-Segel Models

Throughout the literature it is most common, when attempting to model the behaviour of chemotactic bacterial populations (such as chemotactic band formation), to consider a mathematical model such as that devised by Keller & Segel [87]. Commonly referred to as the Keller-Segel (or K-S) model, this was originally created for slime moulds but has been successfully applied to bacterial chemotaxis [88]. This model takes a continuum approach and uses two partial differential equations (PDEs) to represent a population density and concentration of some attractant substance across a spatial domain. A generalised version of this model may be written as:

$$\frac{\partial b}{\partial t} = \nabla \cdot (\chi(s)\nabla b) - \nabla \cdot (\xi(s) b \nabla s) + g(b,s) - h(b,s), \tag{2.8}$$

$$\frac{\partial s}{\partial t} = D\nabla^2 s - f(b,s), \tag{2.9}$$

within which $b(x,t)$ represents the population density, $s(x,t)$ the attractant concentration, x is the spatial position, t denotes time, χ is the chemotactic coefficient, g indicates cell growth, h cell death, f indicates degradation of attractant whilst ξ and D are the diffusion coefficients of the bacteria and attractant, respectively. For more detailed information on the impact of the K-S model in this and other applications we recommend the reviews of Horstmann [89, 90].

It is clear upon examination of the literature that the K-S model has been useful within the study of bacterial chemotaxis of cell populations. One of the

in uence the behaviour observed on the macroscale (population) level by incorporating receptor dynamics into a generic population model [96].

solve analytically [104] and thus it does not necessarily lend itself to gaining insight into how certain behaviours emerge.

Other stochastic approaches have also been considered such as Othmer et al. [105] and Rivero et al. [106]. The Rivero et al. [106] (RTBL) model considered a cell population moving either left or right along an infinite one-dimensional line with a constant velocity v (other methods of motility are discussed by Codling et al. [102]). Considering turning probabilities of the form $r_1 = \ _1$ and $r_2 = \ _2$ for left- and right-moving cells, respectively, it can be shown that

based models have been produced which display clear potential but either fail to account for certain processes or suffer from the same model complexity issue as many single cell models.

It is clear that many different approaches have been considered when modelling chemotaxis. Each of these has their own respective advantages and disadvantages. Within the more recent literature, however, a number of these drawbacks have started to be addressed. In particular, MWC modelling has helped to remove significant amounts of complexity from models whilst

Chapter 3

Mathematical Model of E. coli Chemotaxis Signalling

Within this chapter we analyse a recent mathematical model of the E. coli chemotaxis signalling cascade [70]. Firstly, the model is presented alongside a discussion of how it allows for further investigation of intracellular phenomena where other models from the literature do not. A rigorous analysis of the model is then conducted. In particular, we compare a number of functions describing the methylation dependent free-energy (or set energy) of chemoreceptors against experimental data in order to choose the most suitable form for use throughout this thesis. A non-dimensional re-scaling of the model system is then considered. Using this non-dimensional model it is demonstrated that the system of equations possesses just one biologically feasible steady-state that is subsequently shown to be asymptotically stable. Finally, the eigenvalues of

motivation for the use of the Clausznitzer et al. [70] model presented within this work.

Many mathematical models have focused on describing the processes associated with ligand binding and adaptation [39, 40

equations (3.5) and (3.8) as a Monod-Wyman-Changeux (MWC) description of receptor clus-

the mathematical model laid out above to a range of experimental data. This demonstrated that the model represents a detailed enough description of the chemotaxis signalling pathway of E. coli cells as to adequately represent the biological processes involved. Whilst Clausznitzer et al. [70] clearly explored this model in the context of large amounts of experimental data, they provided very little in the way of mathematical analysis. As such, for the remainder of this chapter we shall present a rigorous analysis of this model fo

all take the same basic form

$$h(m) = \quad (m_0 \quad m): \tag{3.12}$$

In this expression is a scaling value and m_0 represents an initial methylation level (in the absence of any ligand). Tu et al. [63] takes $= 2$ and $m_0 = 1$ to give

$$h(m) = 2(1 \quad m); \tag{3.13}$$

whilst Clausznitzer et al. [70] consider $= 0:5$ and $m_0 = 2$, i.e.

$$h(m) = 1 \quad \frac{m}{2}; \tag{3.14}$$

and Shimizu et al. [118] take $= 2$ and $m_0 = 0:5$, giving

$$h(m) = 2 \quad \frac{1}{2} \quad m \quad : \tag{3.15}$$

Each of these functional forms can be compared to experimental data found in the literature [62, 118, 119] as shown in Figure 3.1. In particular, we compare each $h(m)$ function to the range of methylation states possible for each receptor. It is worth noting that each receptor possesses four methylation sites, which leads to a limit of eight methyl groups per receptor dimer and an upper limit of 48 methyl groups for an assistance neighbourhood of 6 receptor dimers.

The experimental data of both Endres et al. [62] and Vaknin & Berg [119] use similar experimental techniques, whereby Tar receptors were genet

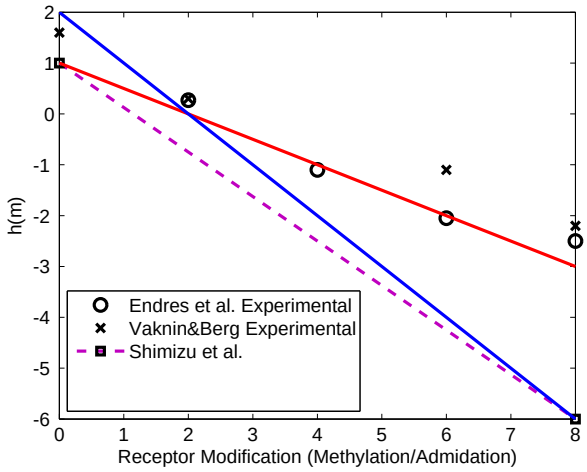
h(m)
Receptor Modification (Methylation/Admidation)
Endres et al. Experimental
Vaknin&Berg Experimental
Shimizu et al.
2
1
0
-1
-2
-3
-4
-5
-6
0
1
2
3
4
5
6
7
8

and from equation (3.20)

$$= \frac{R}{R + B b_p^2} = \frac{1}{1 + \frac{B}{R} b_p^2} = \frac{g_R[R_T]}{g_R[R_T] + g_B[B_T]^2 b_p^2} = \frac{1}{1 + \frac{g_B[B_T]^2 b_p^2}{g_R[R_T]}}: \tag{3.26}$$

Using this expression alongside equation (3.19) we see that

$$e^F = \frac{B}{R} b_p^2 = \frac{g_B[B_T]^2 b_p^2}{g_R[R_T]}; \tag{3.27}$$

within which F is given by equation (3.11). Now, rearranging this equality we are able to obtain the steady-state expression for the average chemoreceptor methylation level

$$\begin{aligned} m &= 2 \left(1 + \ln \left(\frac{1 + [L]/K_a^{off}}{1 + [L]/K_a^{on}} \right) \right) \frac{1}{N} \ln \left(\frac{B b_p^2}{R} \right) \\ &= 2 \left(1 + \ln \left(\frac{1 + [L]/K_a^{off}}{1 + [L]/K_a^{on}} \right) \right) \frac{1}{N} \ln \left(\frac{g_B[B_T]^2 b_p^2}{g_R[R_T]} \right) : \end{aligned} \tag{3.28}$$

Each of the steady-state expressions obtained thus far have been done so by simple rearranging of expressions. These equations may also be utilised to obtain a steady-state expression for a_p (i.e. for equation (3.21)). In this case we substitute the steady-state equations (3.24)-(3.26) into equation (3.21) and multiply through by the denominators of each term. This yields a 5th order polynomial in a_p, the roots of which represent values for a_p. This takes the form

$$p(a_p) = 0 = A a_p^5 + B a_p^4 + C a_p^3 + D a_p^2 + E a_p + F; \tag{3.29}$$

where $A; B; C; D; E$ and F are coefficients of the polynomial $p(a_p)$ that are defined as follows

$$A = g_R[R_T][A_T]^4 k_1 k_2 k_3^3; \tag{3.30}$$

$$\begin{aligned} B = {} & g_B[B_T]^3[A_T]^3 k_2 k_3^3 k_5 - 3 g_R[R_T][A_T]^3 k_1 k_2 k_3^2 k_5 - g_R[R_T][A_T]^3[Z_T] k_1 k_3^3 k_4 \\ & - g_B[B_T]^2[A_T]^3[Y_T] k_2 k_3^3 k_6 - g_R[R_T][A_T]^3[B_T] k_2 k_3^3 k_5 - g_B[B_T]^2[A_T]^3[Y_T][Z_T] k_2 k_3^3 k_4 \\ & - g_R[R_T][A_T]^3[Y_T][Z_T] k_2 k_3^3 k_4 + g_R[R_T][A_T]^4 k_1 k_2 k_3^3 - g_R[R_T][A_T]^3[Y_T] k_2 k_3^3 k_6 \\ & - g_R[R_T][A_T]^3 k_1 k_3^3 k_6; \end{aligned} \tag{3.31}$$

$$\begin{aligned} C = {} & g_B[B_T]^3[A_T]^2 k_3^3 k_5 k_6 + 3 g_R[R_T][A_T]^3 k_1 k_2 k_3^3 k_5 - 3 g_R[R_T][A_T]^2 k_1 k_3^2 k_5 k_6 \\ & - g_R[R_T][A_T]^2[B_T] k_3^3 k_5 k_6 - g_R[R_T][A_T]^2[B_T][Z_T] k_3^3 k_4 k_5 - 3 g_R[R_T][A_T]^2 k_1 k_2 k_3 k_5^2 \end{aligned} \tag{3.32}$$

$2g_R$

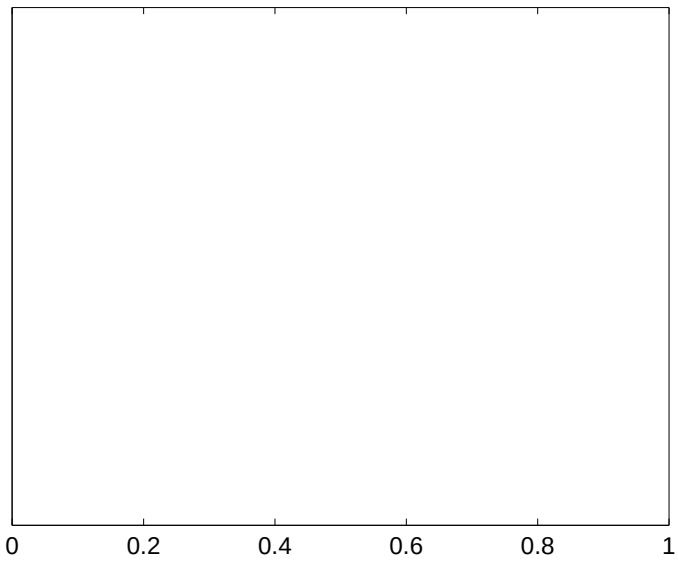
0
0.2
0.4
0.6
0.8
1

$$\frac{\partial f_4}{\partial a_p} = \frac{k_3[A_T](1 \quad b_p)}{k_5}; \tag{3.45}$$

$$\frac{\partial f_4}{\partial b_p} = \frac{k_3[A_T]a_p}{k_5} \quad 1: \tag{3.46}$$

We now investigate the eigenvalues of this system by substituting into the Jacobian each of the steady-state values before solving

$$\det|J \quad I| = 0; \tag{3.47}$$

within which I is the identity matrix with the same dimensions as the Jacobian and denotes an eigen[illegible] values given in Table 3.1 we are able to ob[illegible]

$$_1 = \quad 822{:}1086; \quad _2 = \quad 8{:}8146; \quad _3 [illegible] \quad _4 = \quad 0{:}1942$$

[illegible]r that each of these four eigenvalues of the [illegible]t $_i < 0$ and hence we [illegible]e to conclude that this system is asymptotically [illegible]meter values stated in [illegible].1.

tM[illegible]

adjusts the length of each time step in order to maintain these tolerances as well as the numerical stability of the scheme used.

3.3 Summary & Discussion

Within this chapter we began by presenting a recent mathematical model of the E. coli intracellular signalling pathway from the literature. The remainder of this chapter then sought to produce a rigorous analysis of the model.

This analysis began by examining three different sets of energy functions from the literature in the context of the available experimental data. Upon doing so it was shown that the function of Clausznitzer et al. [70] produced the best fit and will thus be used for all E. coli chemotaxis modelling work in this thesis.

A non-dimensional re-scaling of the model was then presented and utilised in order to demonstrate that there exists just one biologically feasible steady-state for this system. This equilibrium state was subsequently shown to be asymptotically stable, with eigenvalues demonstrating that this is a stiff system.

The analysis conducted within this chapter demonstrates a number of features of this mathematical model that had previously only been assumed within the literature. In addition to this,

Chapter 4

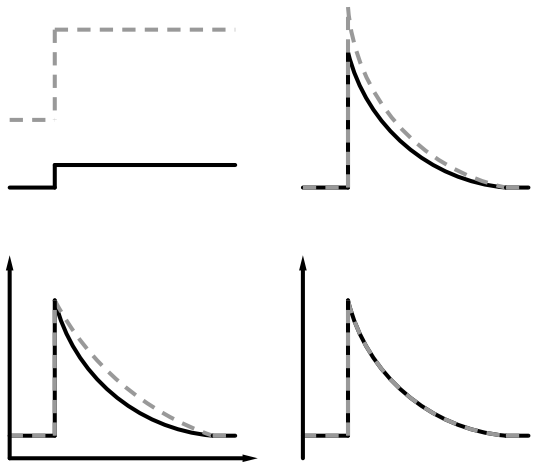

4.2 Conditions for FCD

In this section we outline theoretical conditions required for a mathematical model of the form

$$\underline{x} = f(x(m); ; [L]);$$

which, upon use of the chain rule, is given by

$$\underline{x} = \frac{@x dm}{@m d} = \frac{1}{2} x(m) \frac{dm}{d} = f(x(m); \quad ; [L]): \tag{4.9}$$

The su cient condition given by equation (4.3) may then be tested by multiplying $x(m)$ and $[L]$ by some constant $p > 0$ which gives

$$f(px(m); \quad ; p[L]) = \frac{1}{2} px(m) \frac{dm}{d} = p \quad \frac{1}{2} x(m) \frac{dm}{d} \quad = pf(x(m); \quad ; [L]); \tag{4.10}$$

which clearly satis es equation (4.3).

Examination of equation (

4.3.2 Parameter Sensitivity Analysis

The results of Section 4.3 suggest that the property of FCD will be robust to variation in parameters in the signalling cascade. In order to test this r

Table 4.1: Dissociation constants for active and inactive T

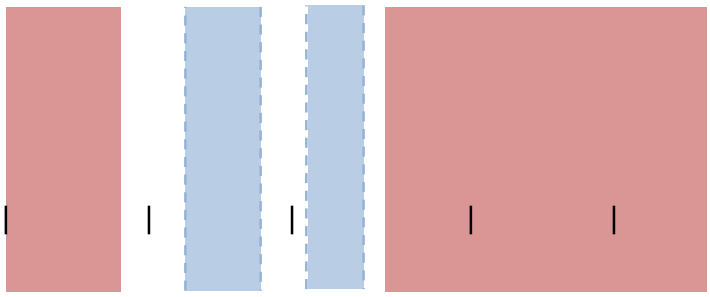

4.4.2 Multiple Di erent Ligand Types

In light of the results of Section 4.4.1 we now consider the e ect of the cell detecting two

[L] K_i^{off} K_i^{on}, K_i^{off} [L] K_i^{on} or K_i^{off} K_i^{on} [L]. Figure 4.8 displays numerical results verifying that FCD holds in this signalling team con guration. It should therefore be biologically feasible given experimentally determined values for the ligand dissociation constants of Tar and Tsr receptors to MeAsp and serine in both cases whether receptors bind either the same or separate ligands.

4.5 Summary & Discussion

Within this chapter we have demonstrated, using both theore

existence of a negative feedback loop in which the protein CheB-P acts to reduce the methylation level of the chemoreceptors. This particular feature of the network is of interest since negative feedback is known to have the potential for creating oscillatory behaviour within monotone dynamical systems (i.e. those in which proteins activating certain processes do not repress that process at a different concentration and vice versa) [134, 135, 136].

Motivated by the existence of this negative feedback loop, we postulate that overshoot can be described as damped oscillatory behaviour. As such, in the remainder of this chapter, we consider the model laid out in Chapter 3 and ask under what conditions it exhibits overshoot.

5.3 Methodology

In this section we consider methods that are needed in order to test the hypothesis stated in Section 5.2. The hypothesis that overshoot may be modelled as damped oscillatory behaviour requires an investigation into how variation in parameter values affect eigenvalues of the system steady-state. Thus we appeal to the theory of asymptotic stability analysis (see Appendix C).

Within Section 3.2.4, an asymptotic stability analysis for the model laid out in Chapter 3 showed that it displays (non-oscillatory) stable behaviour for the parameter values in Table 3.1.

state of a system over some pre-de ned range for any pair of parameters in the system. This stability analysis routine takes the following form.

steady-state and multiplied by 100, giving overshoot amplitude as a percentage of the steady-state value. Other definitions of overshoot amplitude could also have been considered, however, we chose this method so as to allow a fair comparison between our results and those of Min et al. [131].

5.4 Full Four-Dimensional Model Results

Within this section we utilise the numerical routine from Section 5.3

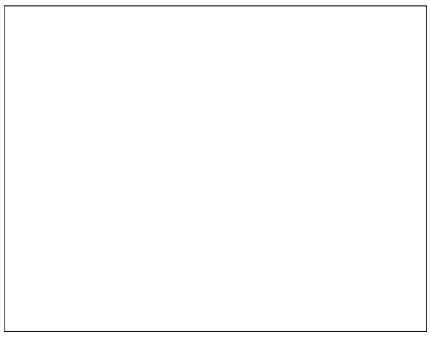

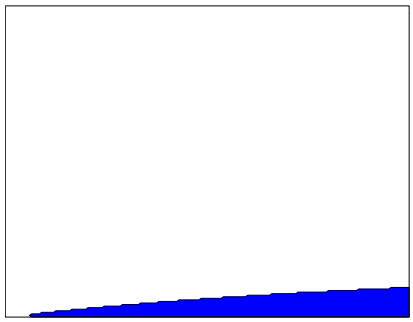

k_2 (

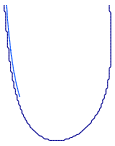

readily than those pairs that included variation of the CheA concentration. Of particular interest amongst the results obtained here is that where the total concentrations of CheB and CheY were varied (see Figure 5.6(d)). In this particular case we note that in order to achieve overshoot,

$$\frac{@r}{@a_p} = \frac{k\ [A_T](1 \quad b_p)}{k} \qquad = \quad ; \qquad (5.12)$$

$$\frac{@r}{@b_p} = \frac{k\ [A_T]a_p}{k} \qquad 1 \qquad = \quad ; \qquad (5.13)$$

are the partial derivatives of equations (5.2)-(5.4) with respect to each of the three system variables. In order to obtain the eigenvalues of the system i

5.5.3 Model 3 - Second-Order System: CheA-P is a Multiple of Receptor Activity

Due to the failure of the second-order model reduction considered in Section 5.5.2 we now investigate an alternative method of reducing this model to a second-order dynamical system. In this particular case we consider the concentration of CheA-P to be a simple multiplicative scaling of the receptor signalling team activity, i.e. $[A_p]$, in which is calculated at steady-state from a numerical simulation of the full system using parameters from Table 3.1 (see Fig. 5.8(c)) and is described by equations (3.9) and (3.11). In addition to this we consider CheY-P to be a decouplable read-out variable as in the model of Tu et al. [63]. This results in a second-order dynamical system of the form

$$\frac{dm}{dt} = \alpha_R(1 - m) - \beta_B b_p = f(m, b_p); \tag{5.24}$$

$$\frac{db_p}{dt} = k_A(1 - b_p) - b_p = g(m, b_p); \tag{5.25}$$

in which is the multiplicative scaling of such that a_p.

In this case the assumption that CheY-P concentration is a (decoupled) output variable means that all phosphoryl groups produced by CheA must transfer to CheB. Clearly this means that the sharing of phosphoryl groups between CheB and CheY has been removed from the system. We can also see that the timescale upon which CheA autophosphorylates has been removed.

Once again, in order to analyse the stability characteristics of this system we must investigate the eigenvalues of the Jacobian matrix. For this particular reduced model the Jacobian matrix is of the form

$$J = \begin{pmatrix} \frac{\partial f}{\partial m} & \frac{\partial f}{\partial b_p} \\ \frac{\partial g}{\partial m} & \frac{\partial g}{\partial b_p} \end{pmatrix}; \tag{5.26}$$

within which the partial derivatives with

Here eigenvalues are obtained upon solving

$$(r_{} + r_{}) + r_{} r_{} \quad r_{} r_{} = 0; \tag{5.31}$$

in which $r_{} r_{}$ are given by equations (5.27)-(5.30). Analysing these eigenvalues shows that a large fold-change (9.5 fold increase) in all protein concentrations is required for this model to display overshoot behaviour, as seen in Figure 5.10. Clearly this represents a significant change from the original fourth-order dynamical system. Thus we conclude that Model 3 does not represent a valid reduction for the system. This supports the notion that the timescales of various reactions in the system as well as the sharing of phosphoryl groups between CheB and CheY are important features in the mechanism causing damped oscillatory behaviour to be observed.

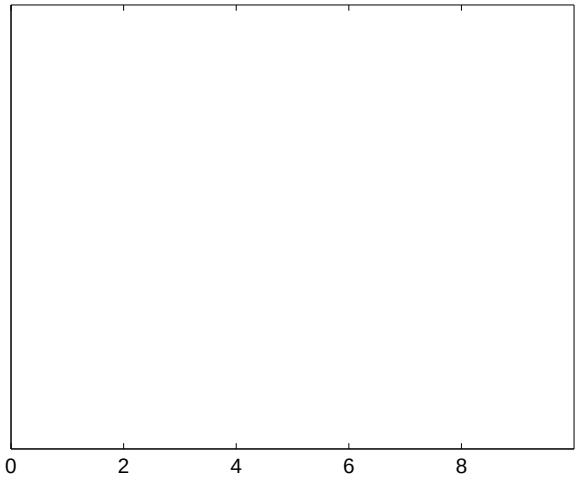

in which is de ned as per equations (3.9) and (3.11) whilst $k_{cat}^{R=B}$ and $K_M^{R=B}$ are catalytic rates and Michaelis-Menten constants of CheR and CheB, respectively. Here the concentration of CheY-P is described by

$$\frac{d[Y_p]}{dt} = k_a \qquad \frac{[Y_p]}{z}; \tag{5.33}$$

in which k_a

5.6 Understanding Key Principles of the Overshoot Response

Using model reduction analysis we have found some support for the idea that the dynamic timescales of intracellular processes are important for the ability of a cell to display overshoot. In order to further examine this, we seek to deduce within this section an analytic expression that is capable of reproducing the region of damped oscillatory behaviour displayed in Figure 5.7.

As discussed in Section 5.5, the use of lower-order dynamical systems may significantly simplify analytical work. Based on the analysis of various reduced model forms, here we shall make use of the third-order reduction considered in Section 5.5.1. Since we seek to explain the emergence of overshoot we must consider here the eigenvalues of the Jacobian matrix for this system, as given by the roots of the characteristic polynomial. In order to do this we consider the different analytical solution forms that may be obtained from a cubic polynomial of the form

$$p(\lambda) = \lambda^3 + A\lambda^2 + B\lambda + C = 0; \qquad (5.s;+s$$

dynamical system, giving the condition

$$\frac{2}{27}\frac{k_2^3[Y_T]^3(1 \quad y_p)^3}{k_5^3} \quad \frac{1}{2}(g_R[R_T] +$$

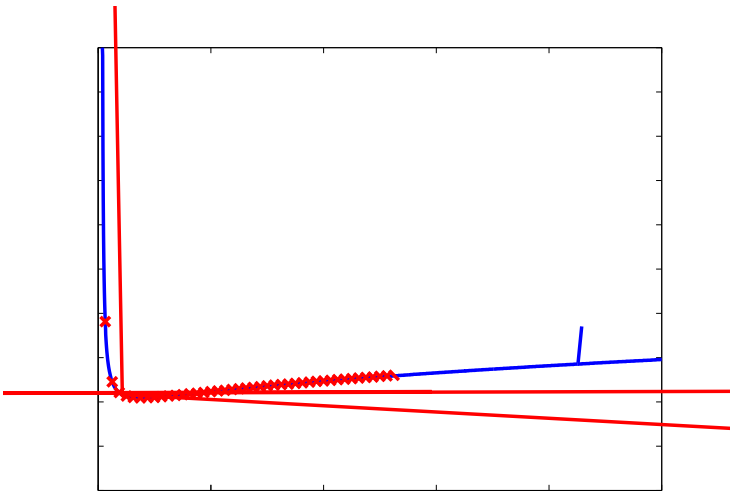

such high fold-changes in protein concentration are often l

the cell has enough time to adapt in both E. coli and Bacillus subtilis [142, 143]. In fact, this observation likely explains the difference between the experimentally obtained results for step-up and step-down stimuli. In the case of a step-up stimulus it is possible for chemoreceptors to become saturated and break apart resulting in neglig 10.9091 Tf 1 0 0 1 447291 7(o(m)272351(3)0.04

have been shown here to be important determinants of the transient cell response. Secondly, simplified mathematical models give a number of benefits, particularly in terms of the ease with which analytical results may be obtained. However, such simplifications not only alter the network structure but the ability of the system to exhibit previously observed transient behaviour as demonstrated in Section 5.5. In particular the ability of the model to fit with biological observations may be greatly altered or lost altogether. One such example is the model due to Tu et al. [63] which has been used with some success in a number of studies such as that by Kalinin et al. [64]

of phenomena including overshoot.

Also, demonstrated here is that protein concentration is an important factor in affecting the temporal response of an intracellular signalling cascade. Based upon the results obtained within this work we believe that there are three key ingredients for determining variation in a network.

2. Update intracellular signalling pathway;
3. Calculate agellar rotational bias;
4. Simulate cell movement - straight swim (run) or turn and swim (tumble);
5. Return to step 1.

For a graphical summary of this algorithm, see Figure 6.1. The details of ABM components 1-4 as well as their respective modelling assumptions and simplications are examined in-depth within

6.1.3 Updating the Signalling Pathway

Within the ABM described here we consider the behaviour of an *E. coli* cell population within the ligand profile and spatial domain discussed in Section 6.1.2. In doing so we describe the response of each individual cell with the model in Chapter 3. The key assumptions and simplifications of this model were discussed in Section 3.1.2.

Within the ABM formulated here, the intracellular signalling cascade ODE model is updated using an inbuilt MATLAB stiff ODE solver (ode15s). In contrast to previous chapters, here we restrict this solver such that it progresses forward by the length of one ABM time-step. This allows a new ligand concentration to be calculated and inputinto the ODE model depending upon the location of each cell.

Using this ODE solver we are able to obtain a complete representation of the internal state of each simulated cell for every model time-step. As such, we are able to observe the response of CheA-P, CheY-P, CheB-P, CheR-bound receptor, methylation level for each cell, and receptor activity

ship. This is given by

$$\text{Bias}_M = \frac{1}{1 + \frac{3}{7}\left(\frac{[Y_p]}{[Y_p]_0}\right)^{5.5}}; \tag{6.4}$$

where $[Y_p]$ is the CheY-P concentration calculated in Section 6.1.3 and $[Y_p]_0$ is the concentration in absence of any stimulus.

Examination of the results in Figure 6.2

that still represents this process to a good degree.

Here we consider the agellar rotational bias expression from Section 6.1.4 (i.e. equation (6.4

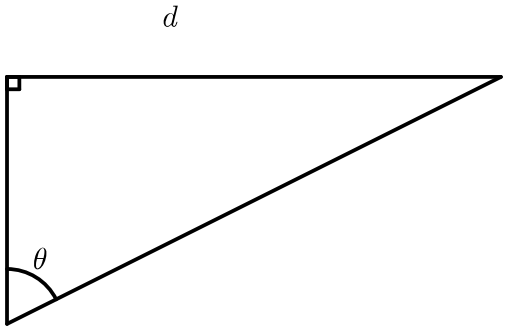
d
θ

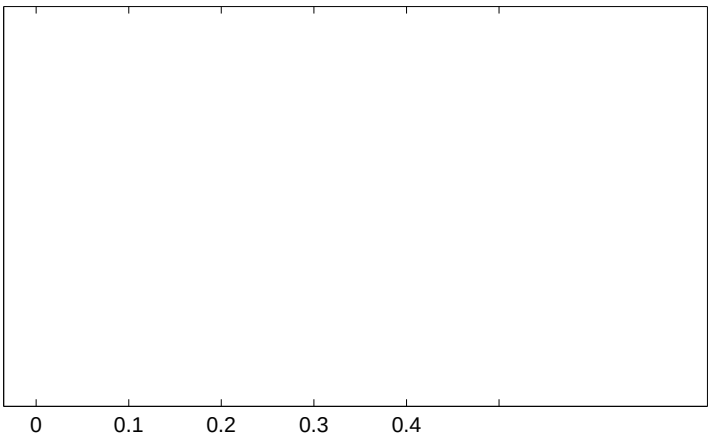
0
0.1
0.2
0.3
0.4

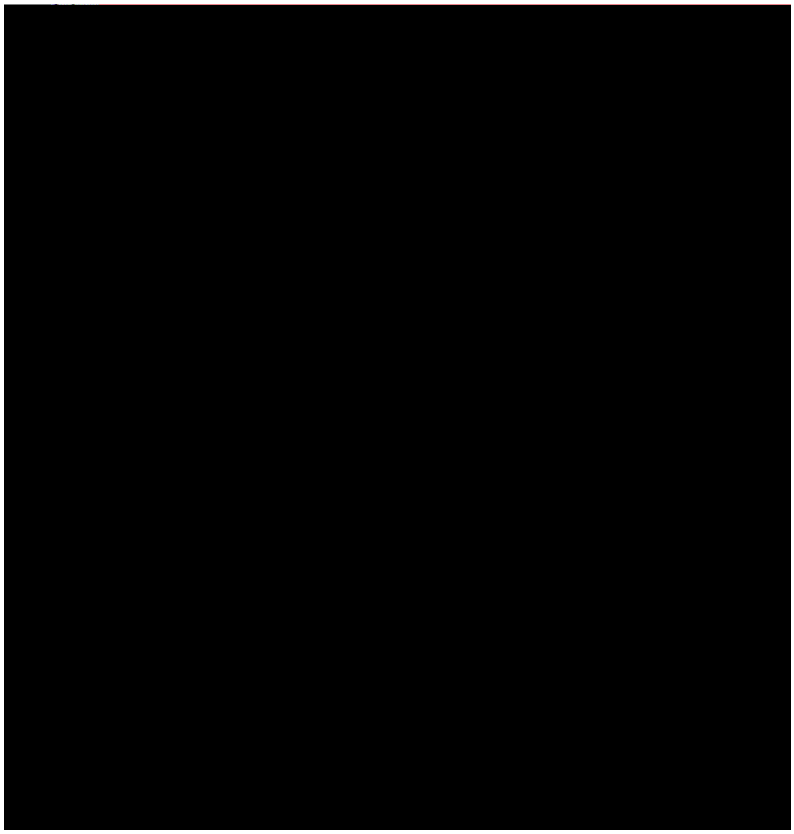

Figure 6.7: Plots showing the typical simulated behaviour of chemotactic E. coli cells in environments containing no spatial ligand heterogeneity (top), a linear MeAsp concentration field (middle) and an exponential MeAsp concentration field (bottom). These results display qualitatively similar behaviour to simulations conducted in the work of Zonia & Bray [109] although an exact comparison is not possible. Note that results shown here represent a typical example selected from a pool of 50 simulated cells in each different ligand gradient.

between results obtained from this ABM and those of another ABM that utilises a similar

understanding of how changes within the signalling networkwill a ect the cell response.

Within this section we have shown that the ABM formulated here cannot be invalidated based upon comparisons with either experimental observations or theoretical results obtained from population level di erential equations and an alternative ABM. None of these tests have displayed results suggesting that the ABM considered here m

lower fractions of phosphorylated proteins at steady-state,

shorter adaptation times,

smaller initial response amplitudes (in terms of phosphorylated fraction),

than those with smaller total protein concentrations. Such variation in total protein concentrations is then applied in the signalling pathway ODE model from Chapter 3 which is used to simulate the behaviour of *E. coli* cells in the ABM.

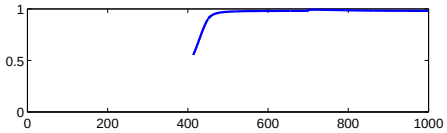

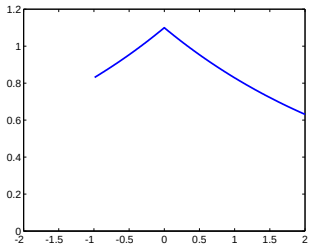
1.2
1
0.8
0.6
0.4
0.2
0
-2
-1.5
-1
-0.5
0
0.5
1
1.5
2

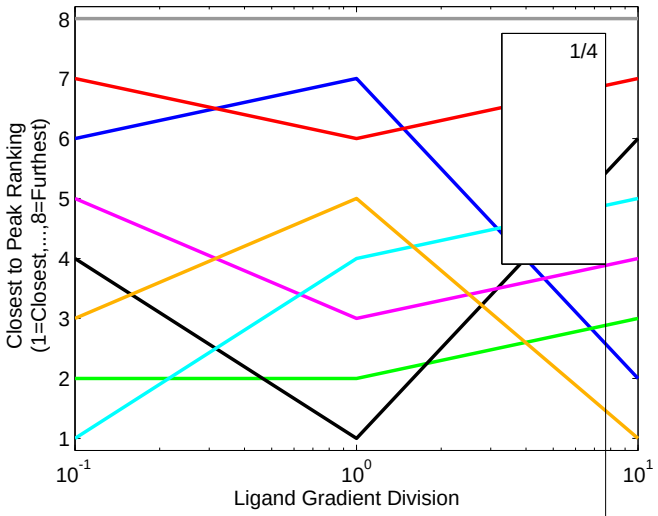
1/4
Closest to Peak Ranking
(1=Closest,...,8=Furthest)
Ligand Gradient Division
8
7
6
5
4
3
2
1
10^-1
10^0
10^1

shown that for small to intermediate MeAsp concentrations, the e ect of MeAsp binding to Tsr receptors is negligible (see Figure 4.7(a)) and as such this e ect has previously been ignored. However, by considering a slight adjustment to equation (3.10) it is possible to incorporate MeAsp and serine binding to Tar and Tsr receptors, respectively. This results in a free-energy expression of the form

$$F = N\left[1 + \left(\frac{m}{2} + \alpha_a \ln\left[\frac{1 + [L_a]/K_a^{off}}{1 + [L_a]/K_a^{on}}\right] + \alpha_s \ln\left[\frac{1 + [L_s]/K_{ser}^{off}}{1 + [L_s]/K_{ser}^{on}}\right]\right)\right]; \qquad (6.10)$$

within which $[L_a]$ and $[L_s]$ represent the concentrations of MeAsp and serine, respectively while $K_{ser}^{on} = 1\,\text{mM}$ and $K_{ser}^{off} = 0.0025\,\text{mM}$ denote the ligand dissociation constants of Tsr chemoreceptors to serine in their active and inactive states, respectively [69]. In addition to this α_a and α_s denote the abundance ratio of the two chemoreceptor types, defined as $\alpha_a : \alpha_s = 1 : 277.$ 75155(e)-30

K7393(o)0

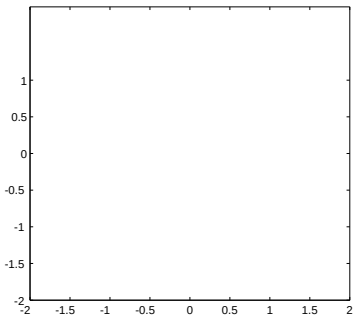
1
0.5
0
-0.5
-1
-1.5
-2
-2
-1.5
-1
-0.5
0
0.5
1
1.5
2

a single response. In order to consider the ability of cells to accumulate about serine we look to Figure 6.14. It is clear from these results that the value at which cells begin to accumulate toward MeAsp is fairly similar in each of the three examples. This would suggest that a ligand

toward a ligand concentration for which they are most sensitive rather than the largest absolute concentration. In the case of two competing gradients it is necessary to compare the sensitivity of cells to each in order to assess which gradient will be preferred, with some intermediate regime in which some cells will be attracted to the peak of each gradient.

The results discussed within this chapter demonstrate some of the potential uses of ABM in the study of bacterial chemotaxis. In fact, they would tend to suggest that approaches such as

Chapter 7

R. sphaeroides Chemotaxis Signalling

In this chapter we investigate the chemotaxis signalling pathways of R. sphaeroides cells. We

for adaptation. They also went on to state that in spite of utilising homologues of the same proteins, the mechanism for adaptation in *R. sphaeroides* does not appear to be the same as that of *B. subtilis* or *E. coli*.

Recently, the work of Hamadeh et al. [176] and Kojadinovic et al. [161] demonstrated the existence of fold-change detection (FCD) within chemotactic *R. sphaeroides* cells. The theoretical work of Kojadinovic et al. [161] is of particular interest here since it extends the work of Tindall et al. [174] and couples this with an MWC-based adaptation mechanism similar to those considered for *E. coli* chemotaxis modelling for both the polar and cytoplasmic receptor clusters. This model therefore represents the most complete description of the chemotaxis signalling pathways of *R. sphaeroides* within the literature.

7.2 Motivation

Since the work summarised in Section 7.1, new experimental data has become available that has sought to provide new insight into the chemotaxis signalling pathways of *R. sphaeroides* cells [162]. In particular, this work examined the effects on chemotactic swimming behaviour of various different cellular mutations (alterations from the

It is clear from Section 7.1 that a number of mathematical models have been used to study certain features of R. sphaeroides

complete model to date does not represent an adequate descri

cluster activity ($_C$) is also borrowed from *E. coli* and is described by the expression

$$_C = \frac{1}{1 + e^{F_C}}; \tag{7.4}$$

in which F_C represents the free-energy of a cytoplasmic cluster chemoreceptor signalling team. This free-energy is represented by

$$F_C = N_C \left[1 \quad \frac{m_C}{2} + \ln \quad \frac{1 + [L]/K_C^{off}}{1 + [L]/K_C^{on}} \right]; \tag{7.5}$$

where N_C indicates how many receptors constitute a signalling team within the cytoplasmic cluster, [L] is the ligand concentration, $K_C^{on/off}$ are the ligand dissociation constants of cytoplasmic cluster chemoreceptors in their active and inactive states, respectively and m_C is the methylation level of the cytoplasmic chemoreceptors. The dynamic behaviour of the chemoreceptor methylation level is given by

$$\frac{dm_C}{dt} = g_{R3}$$

Table 7.2: A base set of *R. sphaeroides* parameter values from experimental and theoretical literature sources. Here the superscript a denotes a value taken directly from experimental data, b shows that a parameter was obtained by fitting a mathematical model to experimental data and c indicates that a value was inferred from *E. coli* experimental values.

Symbol	Description	Value	Source
k_r	Rate of CheA autophosphorylation	$0.12\,s^{-1}$	[177][a]
k	Rate of CheA phosphorylation by CheA	Ra4	

and conservation laws may also be applied to the reactions involving CheY proteins, yielding the following ODEs for the behaviour of CheY$_3$-P, CheY$_4$-P and CheY$_6$-P. These are of the form

$$\frac{d[Y_{3p}]}{dt} = k_3[A_{2p}]([Y_3]_T - [Y_{3p}]) - k_{-3}[Y_{3p}]([A_2]_T - [A_{2p}]) - k_{10}[Y_{3p}]; \quad (7.9)$$

$$\frac{d[Y_{4p}]}{dt} = k_4[A_{2p}]([Y_4]_T - [Y_{4p}]) - k_{-4}[Y_{4p}]([A_2]_T - [A_{2p}]) - k_{11}[Y_{4p}]; \quad (7.10)$$

$$\frac{d[Y_{6p}]}{dt} = k_5[A_{2p}]([Y_6]_T - [Y_{6p}]) + k_8[A_{3p}]([Y_6]_T - [Y_{6p}]) - k_{-8}([A_3]_T - [A_{3p}])[Y_{6p}] - k_{12}[Y_{6p}] - k_{15}([A_3]_T - [A_{3p}])[Y_{6p}] - k_{16}[A_{3p}][Y_{6p}]; \quad (7.11)$$

26.37227(i)-1.02498(n)]TJ (E)-0.62420.202-397.987(m)-0.250651(a)2p950013(E)-0492351(l)-1.8.1088(y)-39492351(l)-1.024
l])[A]]Y 16 T]6pTJ /R8445 744(e)-273.767s /R445682(w 7.97613J /R461 10.9091 Tf 35(o)0J /R11740389(f)R445366)0.124207(s)-(i)-1.02498(n)-0.22gbel

7.4 Model Analysis

7.4.1 Non-Dimensionalisation

Here we consider a non-dimensionalisation (re-scaling) of the mathematical model presented in equations (7.1)-(7.13). In particular we make the choice to re-scale each of the chemotaxis protein concentrations with respect to the relevant total concentration, eg. $[A_{2p}$

within which lower case a_i $(i = 2;3)$, y_i $(i = 3;4;6)$ and b_i $(i = 1;2)$ denote the (non-dimensional) fractions of the relevant chemotaxis proteins that are phosphorylated, k_i

Those conditions for variables m_P and m_C

arrange these two expressions in order to obtain the steady-state expressions for the average chemoreceptor methylation level at the polar and cytoplasm

$$c_r = 3{:}3667\ \ 10\ \ + 4{:}4652\ \ 10\ \ a_p + 2{:}2002\ \ 10\ \ a_p + 3{:}0993\ \ 10\ \ a_p \quad (7.50)$$

$$+\ \ 7{:}9690\ \ 10\ \ a_p;$$

where each term is expressed to four decimal places. Examining these values shows that in the range $0 \quad a_p \quad 1$ coefficients c_r -c_r are negative whilst c_r is positive. Coefficient c_r may be either positive or negative depending upon the magnitude of a_p. In spite of the fact that the sign of c_r may change it is clear that there exists just one sign change between consecutive polynomial coefficients. Hence there will be just one positive steady-state value for this equation. Furthermore we may examine the coefficients of the polynomial $q(a_p; \ a_p)$, within which the coefficients c_r , c_r and c_r will take the opposite sign to the previous case. As such we find that there are four changes in sign between consecutive polynomial coefficients. It will therefore be the case that this polynomial will have either:

Case i: one positive real, four negative real and zero complex roots;

Case ii: one positive real, two negative real and two complex roots; or

Case iii: one positive real, zero negative real and four complex roots.

However, in each of the above three cases these four roots are not biologically feasible and as such they may be neglected.

Analysis of the coefficients in the polynomial equation (7.43) using Descartes' rule of signs is inconclusive, i.e. the signs of the coefficients are not all

given by

$$J = \begin{pmatrix} \frac{\partial g_1}{\partial m_1} & 0 & 0 & 0 & 0 & 0 & 0 & \frac{\partial g_1}{\partial b_1} & 0 \\ 0 & \frac{\partial g_2}{\partial m_2} & 0 & 0 & 0 & 0 & 0 & 0 & \frac{\partial g_2}{\partial b_2} \\ \frac{\partial g_3}{\partial m_1} & 0 & \frac{\partial g_3}{\partial a_1} & 0 & \frac{\partial g_3}{\partial \gamma_1} & \frac{\partial g_3}{\partial \chi_1} & \frac{\partial g_3}{\partial \gamma_1} & \frac{\partial g_3}{\partial b_1} & \frac{\partial g_3}{\partial b_2} \\ 0 & \frac{\partial g_4}{\partial m_2} & 0 & \frac{\partial g_4}{\partial a_2} & 0 & 0 & \frac{\partial g_4}{\partial \gamma_2} & 0 & \frac{\partial g_4}{\partial b_2} \\ 0 & 0 & \frac{\partial g_5}{\partial a_1} & 0 & \frac{\partial g_5}{\partial \gamma_1} & 0 & 0 & 0 & 0 \\ 0 & 0 & \frac{\partial g_6}{\partial a_1} & 0 & 0 & \frac{\partial g_6}{\partial \chi_1} & 0 & 0 & 0 \\ 0 & 0 & \frac{\partial g_7}{\partial a_1} & \frac{\partial g_7}{\partial a_2} & 0 & 0 & \frac{\partial g_7}{\partial \gamma_1} & \frac{\partial g_7}{\partial b_1} & \frac{\partial g_7}{\partial b_2} \\ 0 & 0 & \frac{\partial g_8}{\partial a_1} & 0 & 0 & 0 & 0 & \frac{\partial g_8}{\partial b_1} & 0 \\ 0 & 0 & \frac{\partial g_9}{\partial a_1} & \frac{\partial g_9}{\partial a_2} & 0 & 0 & 0 & 0 & \frac{\partial g_9}{\partial b_2} \end{pmatrix} : \quad (7.51)$$

$$\frac{@g}{@a_p} = \quad k \quad _C \quad k_8(1 \quad y_{\,p}) \quad k \quad _8 y_{\,p} \quad k_9(1 \quad b_{\,p}) \quad k \quad _9 b_{\,p}; \tag{7.64}$$

$$\frac{@g}{@y_p} = k_8 a_{\,p} + k \quad _8(1 \quad a_{\,p}); \tag{7.65}$$

$$\frac{@g}{@b_p} = k_9 a_{\,p} + k \quad _9(1 \quad a_{\,p}); \tag{7.66}$$

$$\frac{@g}{@a_p} = \quad _r k\,(1 \quad y_{\,p}) + \quad _r k \quad y_{\,p}; \tag{7.67}$$

$$\frac{@g}{@y_p} = \quad _r k\, a$$

and as such damped oscillatory behaviour is likely a fixed feature of this system under realistic conditions.

7.4.4 Model Stiffness

As discussed in Section 3.2.5

Table 7.4: Alterations to kinetic rates required for the creation of each *R. sphaeroides* chemotaxis mutant model used in this chapter.

Strain	Parameters set to zero	Other
#1	No alteration	-
#2	k_{-}, k_{-}, k_9, k_9, k_{-}, g_B	$b_p = 0$
#3	g_R	-
#6	k	

Table 7.5: Steady-state values for CheY-P, CheY -P and CheY -P in a number of R. sphaeroides

Chapter 8

Understanding p ro using Simpli ed Modelling Approaches

Within this chapter we further investigate mechanisms associated with chemotaxis in R. sphaeroides. In particular, we formulate and analyse two simpli ed mathematical models in order to elucidate the workings of various system components. Firstly, we formulate a simple model of the cytoplasmic cluster in order to understand the roles of processes acting there. We then consider a simpli ed Kojadinovic et al. [161] model, in which adaptation is removed. This is rst used to verify that the correct intracellular re actions are considered regardless of whether or not adaptation mechanisms are included. In addition to this, the creation of various models based on mutations considered within the experimental data allows us to further our understanding of the cell's agellar response. This chapter concludes with the proposal of a

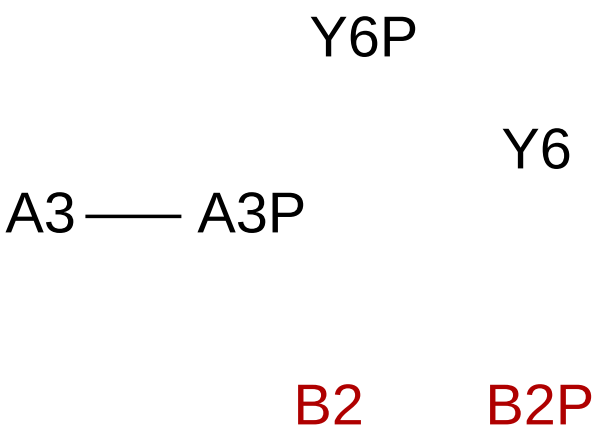
Y6P
Y6
A3
A3P
B2
B2P

Here, k_i $(i = 8; \quad 8; 9; \quad 9; 12; 14; 15;$

signalling teams. This yields the non-linear ODEs

$$\frac{d[A_p]}{dt} = k_{r\_P}([A]_T - [A_p]) - k[A_p]([Y$$

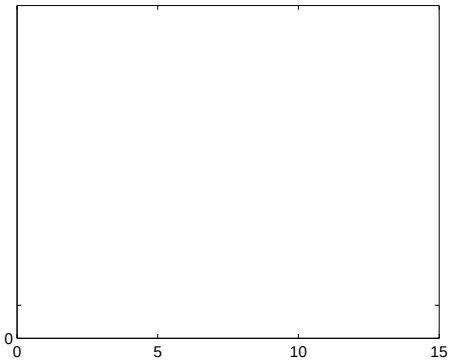
0
0
5
10
15

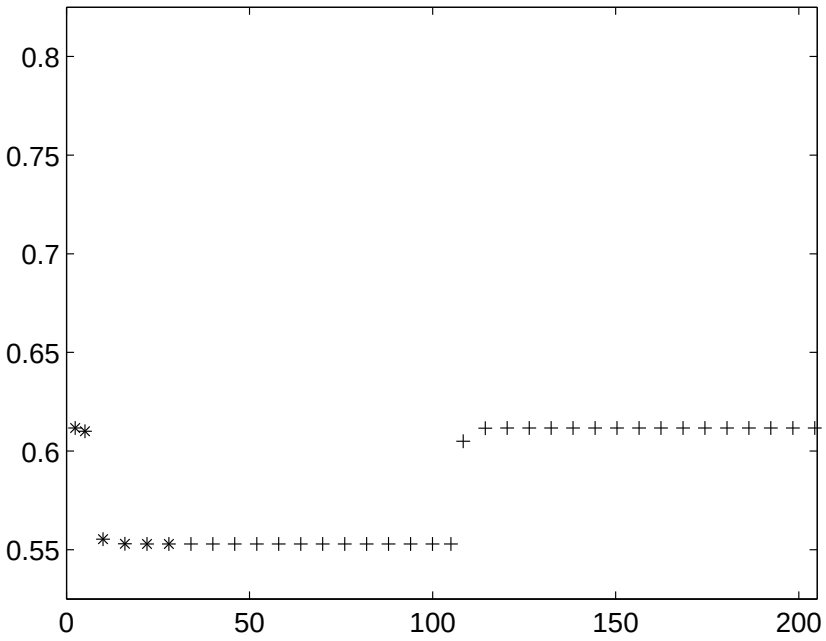
0.8
0.75
0.7
0.65
0.6
0.55
0
50
100
150
200

Considering steady-state and dynamic results together, we

The results presented within this section clearly demonstrate the roles of each cytoplasmic cluster process. Whilst useful in its own right, this model considers only the cytoplasmic cluster. Thus, in order to improve our understanding of other cell features it is necessary to consider the two chemosensory pathways together in the same model.

8.3.2 Validation of the Signalling Pathways

In Section 8.3.1 a simplified mathematical model of processes occurring at the cytoplasmic cluster in *R. sphaeroides* cells was investigated. Studying the steady-state and dynamic properties of this simplified ODE model with various processes systematically removed allowed us to assign likely roles to each of the relevant signalling proteins acting at the cytoplasmic cluster. Within this section we utilise Simplified Model 2 (Section 8.2.2) in order to investigate a key outstanding question relating to the polar cluster. This is as follows.

> A reverse phosphotransfer from CheB-P onto CheA has been observed *in vitro* experimental work. However, to date, this has not been shown to occur *in vivo*. Would we expect to see this reaction occurring?

Within the previous literature, all phosphorylation reactions included within the Kojadinovic et al. [161] model have been shown to occur *in vitro*. In fact, all apart from the reverse phosphotransfer from CheB-P onto CheA have also been demonstrated to exist *in vivo*. An investigation into the existence of this reaction allows us to create a full, validated set of phosphorylation/dephosphorylation reactions occurring within *R. sphaeroides* cells. This is explored in-depth within the next section.

Is Reverse Phosphotransfer from CheB2-P onto CheA2 Expected *in vitro*?

As discussed in Section 8.3.2, all phosphorylation/dephosphorylation reactions in the signalling pathways of *R. sphaeroides* cells have been validated except for one. This is the reverse phosphotransfer from CheB-P onto CheA which has been shown to be possible *in vitro* but not demonstrated *in vivo*. As such, here we utilise exwa ect.ost utili-0.675863(34(h)-0.22496(38

Using a steady-state analysis of the two systems discussed here, the effects of a reverse phosphotransfer from CheB-P onto CheA can be investigated. In particular, the differences between the steady-states of each signalling protein can be studied, which should allow a prediction to be

this process is acting to limit the CheB -P concentration.

8.3.3 Understanding the Motor Response

Within this section we seek to elucidate mechanisms underly

Table 8.3: Steady-state CheY concentrations for wild-type and CheY$_{;}$ cell types. All concentrations listed in this table are expressed in M and are shown to four decimal places.

Cell Type	[CheY -P]	[CheY -P]	[CheY -P]
W-T	5.27087 10	5.2514	68.9646
CheY$_{;}$	0	0	68.1697

the steady-state concentration of CheY-P. In fact, this particular mutation only leads to an increase of 0:8 M (of the total 225 M) in the steady-state CheY -P concentration. We would anticipate that this small increase would not be su ci ent to allow for the experimentally observed behavioural di erences if CheY-P dominantly controls agellar rotational behaviour. Thus, we must consider what is the cause of this behavioural iderence if it is not a di erence in CheY -P concentration?

One possible cause of the di erence between W-T and CheY$_{;}$ cells is that the agellar motor of R. sphaeroides

How is Flagellar Rotation Controlled?

In this section we consider a number of alterations to Simplified Model 2 (Section 8.2.2), each of which represents one of the mutant cell types described in Table 7.1. In order to investigate how the flagellar rotational behaviour is controlled we conduct steady-state analyses of each mutant model. This, alongside the experimental data of de Beyer [162] (Figure 7.2) then allows us to investigate how protein phosphorylation levels act to control the flagellar rotational behaviour.

Table 8.4: Kinetic rate alterations required to create each *R. sphaeroides* mutant model.

Strain	Parameters set to zero	Other
#1	No alteration	-
#2	|	-
#3	|	-
#4	k k k k	-
#5	P	-
#6	k k k k P	-
#7	k k_8 k_{-8} k_9 k_{-9} k_r k_r k_r C	$y_p = 1$
#8	k k_8 k_{-8} k_r k_r k_r C	$y_p = 1$
#9	k k k_r	$y_p = 0$
#10	k k $k_{r,r}$	$y_p = 0$
#11	k k k k k_r $k_{r,r}$	$y_p = 0 = y_p$
#12	k k k k k_r $k_{r,r}$	$y_p = 0$
#13	k k k k k_r $k_{r,r}$	$y_p = 0 = y_p$
#14	k k k k k_r $k_{r,r}$	-
#15	|	-
#16	|	-
#17	|	-
#18	|	-
#19	|	-
#20	k_{-8} k_{-9} C	-
#21	C	-
#22	k k_8 k_{-8} k_r k_r k_r	$y_p = 0$
#23	k k k_r	$y_p = 1$
#24	k k $k_{r,r}$	$y_p = 1$
#25	k k k k k_r $k_{r,r}$	$y_p = 1 = y_p$
#26	k k k k k_r $k_{r,r}$	$y_p = 1$
#27	k k k k k_r $k_{r,r}$	$y_p = 1$
#28	k k k k k k_8 k_{-8} k_r $k_{r,r}$ k_r k_r k_r	-
#29	k k_8 k_{-8} k_r k_r k_r	$y_p = 1$
#30	k k $k_{r,r}$	-
#31	k k k_r	-
#32	k k_8 k_{-8} k_r k_r k_r	-

Similar to the work in Section 7.5, here we implement a number of changes to model parameters in order to represent each mutant cell type. These are detailed in Table

Table 8.5: Steady-states of each *R. sphaeroides*

Table 8.6: Eigenvalues associated with the steady-state of

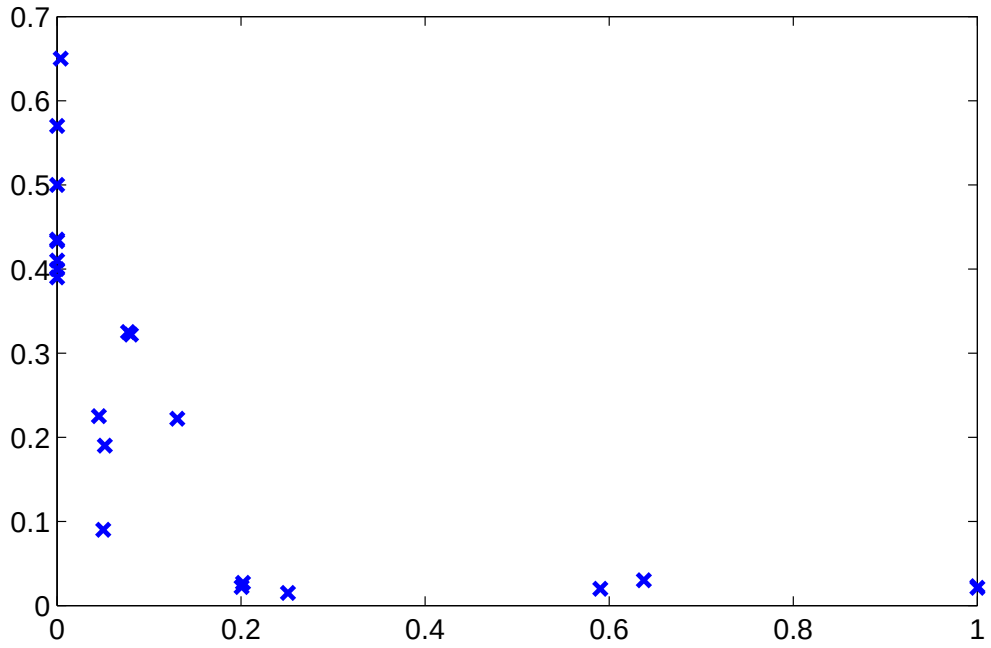
0.7
0.6
0.5
0.4
0.3
0.2
0.1
0
0
0.2
0.4
0.6
0.8
1

Based on these suggestions we must now propose a mechanism for the cytoplasmic cluster that relieves the issue of CheY-P saturation when CheB is deleted from the cell and also allows for the sensing of a metabolic signal (see Figure 8.6). In order to do this we look to the simplified cytoplasmic cluster model considered in Section 8.2.1. This mechanism clearly solved the issue associated with the deletion of CheB and is easily adjusted to consider metabolic signals. As such, here we utilise the law of mass action (see Appendix A), conservation laws and a non-dimensionalisation similar to those in Section 7.4. This yields the set of non-dimensional ODEs

$$\frac{dm_P}{d} = {}_R(1 \quad {}_P) \quad {}_{B^r}b_p \quad {}_P; \tag{8.18}$$

$$\begin{aligned}\frac{da_p}{d} = {}& {}_P(1 \quad a_p) \quad k\,a_p(1 \quad y_p) + k \quad (1 \quad a_p)y_p \quad k\,a_p(1 \quad y_p) \\ & + k \quad (1 \quad a_p)y_p \quad k\,a_p(1 \quad y_p) \quad k\,a_p(1 \quad b_p) + k \quad (1 \quad a_p)b_p \\ & k_r a_p(1 \quad b_p) + k_r(1 \quad a_p)b_p;\end{aligned} \tag{8.19}$$

$$\frac{a_p}{d} = k \quad {}_C(1 \quad a_p)$$

$$y_p = y_p \; ; \quad \bar{b}_p = \bar{b}_p \quad \text{and} \quad b_p = b_p :$$

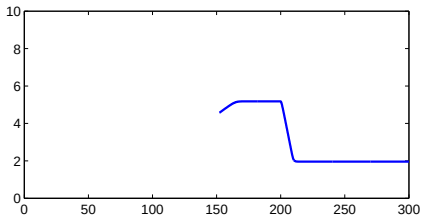
10
8
6
4
2
0
0
50
100
150
200
250
300

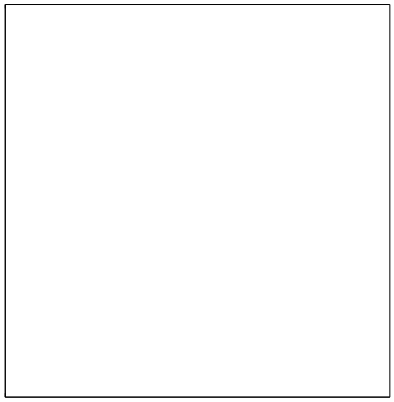
0

have been examined. In doing so a number of features of the signalling pathway have been investigated. Speci cally, steady state analyses of these

behaviour of R. sphaeroides cells. In support of this idea it was shown that the relative concentration of CheY -P against the cumulative concentration of proteins CheY -P and CheY

Chapter 9

Discussion

The main achievements of the work in this thesis have been the analyses of ODE models of *E. coli* and *R. sphaeroides* chemotaxis signalling pathways.

In particular, analysis of the *E. coli* ODE model system revealed key features associated with the phenomena of fold-change detection (FCD) and overshoot. These studies illustrated the importance of receptor dynamics, methylation and phosphorylation timescales as well as total protein concentrations. Further to this, agent-based modelling allowed an investigation in to the effects of these features/phenomena upon the overall behaviour of a cell population to be investigated.

Analysis of the *E. coli* chemotaxis signalling network equipped us with a number of tools that were used in order to study the more complex *R. sphaeroides* system. This allowed us to assign roles to a number of signalling proteins as well as identifying areas that require improvement within future work.

Here we summarise the main findings of this work in addition to giving areas for future theoretical and experimental work. This will help to further elucidate the signalling cascade characteristics of *E. coli* and *R. sphaeroides* as well as other biological systems.

9.1 Summary & Conclusions

In Chapter 2 we provided a summary of the past literature most relevant to the work contained within this thesis. In particular, we began by summarising the biological work that sought to identify key components of chemotaxis signalling cascades and their respective roles. Additionally, throughout this chapter we focused on how experimental results inspired mathematical modelling and vice versa, leading to the modern understanding

an ABM framework in order to investigate *E. coli* population level phenomena. Using the ABM we were able to extrapolate single cell findings to study the effect of variation in protein concentration on the efficiency of the chemotactic response within ligand gradients of varying steepness. Also considered here was the ability of cells to perform chemotaxis when two separate

used within a recent experimental study (neglecting those relating to CheR and CheB proteins associated with adaptation). Within this work it was possible to show that a model without

9.2.1 Modelling Assumptions

Within this thesis a number of di erent mathematical models have been formulated and

ter. In order to understand how spatial organisation such as this affects the cell's chemotactic response, it is possible to use a PDE model. This would allow of the consideration of protein diffusion within the cytoplasm as well as restriction of certain components to specific regions of

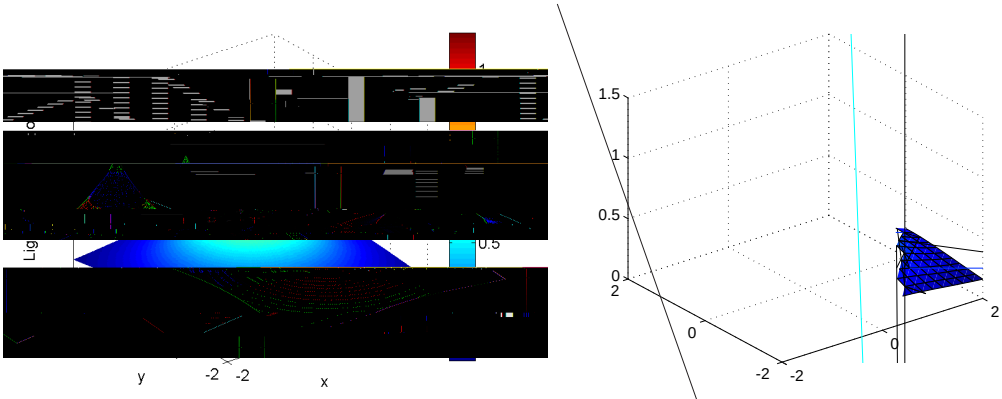

(a) Exponential ligand pro le

cells in a xed, exponential ligand eld over a time period of 12 minutes requires 45 minutes

ABM simulation is completed for some region of interest. This has the potential to significantly reduce computational costs; however a significant amount of work would be required to allow the matching of results between the two different simulation regions/regimes.

9.2.3 *Improved model of adaptation*

In Chapters 7 and 8 of this thesis, the chemotaxis signalling pathways of *R. sphaeroides* cells were our focus. In spite of being able to show that the ODE model of the phosphotransfer network appears, in the most part, to re-produce experimental data the adaptation mechanisms included in the modelling work were shown to be inadequate. As such, a new modelling approach is required in order to fully explain this data. There are a number of ways in which a new mathematical model of adaptation could be formulated, a few of which shall be briefly summarised here.

d[L]=dt = 0). Using currently available experimental techniques it is possible to experimentally determine both d =dt and @ =@m As such, we could then formulate a functional description of the methylation/demethylation ODE (dm=dt) that provides a good t to the experimental data.

9.2.4 Experimental Work

We have so far discussed a number of assumptions and limitations associated with the work in this thesis. Another key area in which further work would help to improve our knowledge of chemotaxis signalling is through comparison of results from this work with theory and new

cells in which the total concentration of all signalling proteins may be controlled. In addition to this it would be necessary to create a well-controlled ligand gradient that very closely matches those in our ABM simulations. These newly created cells could then be placed into the controlled ligand gradient. Observing their behaviour over time, it should then be possible to compare the migration of cells in this experimental work to our ABM simulations, thus either confirming or invalidating this work.

In conclusion, a number of phenomena associated with chemotaxis of *E. coli* cells have been investigated. It is hoped that the modelling framework/methodology, observations and predictions within this work will be useful to future work on bacterial chemotaxis and other biological systems. In the case of *R. sphaeroides* a number of areas have been identified that would benefit from further theoretical and experimental work. In addition to this, a new model was postulated that helps to remove some of the issues of previous models. As such it is hoped that this work proves a useful step in providing a more complete understanding of chemotaxis in *R. sphaeroides* asslIAswsgnalling 9ework i1575155(e)-0.3837(4(d0.226034(e)-0.675863(m)-0.2506

Appendix B

Descartes' Rule of Signs

Descartes' rule of signs may be used to investigate solutions of polynomial equations. More specifically it may be used to find the number of positive, negative and complex roots that can possibly be obtained from a polynomial equation.

In order to utilise this rule it is first necessary to arrange the polynomial equation in order from highest to lowest power of the relevant variable, for example

$$p(x) = a_r x \quad a x \quad a x \quad a = 0; \tag{B.1}$$

within which x is the variable of interest and a_i $(i = 1; 2; 3; 4)$ are the polynomial coefficients expressed such that every $a_i > 0$, i.e. the relevant signs should be expressed in the equation rather than hidden in the coefficient definitions. It is then possible to apply Descartes' rule of signs in two main forms (Rule 1 and Rule 2), which are as follows.

> Rule 1: For a polynomial equation $p(x)$ with real coefficients, the maximum number of positive real roots of this equation will be equal to the number of sign changes in the coefficients (with zero coefficients not constituting a sign change). Then, the number of positive real roots will either be equal to this maximum or will be less than this by some

Rule 3: It is also sometimes possible to obtain some information about the minimum

and so there will exist one negative, real root to the polynomial equation (B.4).

In order to use Rule 3 we may then see that $q = 0$ and $r = 1$, from above. We may then calculate that there will be two complex roots since $n - (q + r) = 3 - (0 + 1) = 2$.

Appendix C

Appendix D

Protein Synthesis

Within Chapter 5 it was discussed that there exists a significant amount of variation in the concentrations of signalling proteins in *E. coli* cells. One of the causes of this is the stochastic nature of gene expression which has been studied in some depth for *E. coli* cells. Here we briefly summarise the process by which proteins are synthesised within cells.

Appendix E

FCD in a Model with Multiple

where all symbols retain their earlier de nition. Substitu ting this into equation (3.9) gives

$$= \frac{1}{1 + \frac{[L]^R}{x(m)}^N}; \qquad \text{(E.4)}$$

where $R = {}_a + {}_s$ and $x(m) = K^{off}$

Glossary

Adaptation

The process by which cells return to a pre-stimulus state. In the case of *E. coli* this occurs

however a number of strains that may cause illnesses such as gastroenteritis, urinary tract infections and neonatal meningitis.

Eukaryote

A type of cell that contains a membrane-bound nucleus.

Flagellum (Plural: Flagella)

A long, slender, whip-like extension of a cell used for movement. The rotational movement

Methylation (Demethylation)

The addition of methyl groups onto, for example, a chemoreceptor is referred to as methylation. Demethylation relates to the removal of methyl groups.

Methylesterase

A protein that is able to remove methyl groups from chemoreceptors. This plays a key role in the process of adaptation.

Prokaryote

A single-cell organism lacking a distinct nucleus.

Receptor Cluster

A number of chemoreceptors that are closely packed in an area. This is often necessary to enhance the sensitivity of a cellular response.

Response Regulator

The protein controlling the response of the cell. For *E. coli* the response regulator (CheY) controls the swimming behaviour of the cell.

Rhodobacter sphaeroides (*R. sphaeroides*)

Bibliography

[13] E. Kort, M. Goy, S. Larsen, and J. Adler. Methylation of a membrane protein involved in

[49] D. Bray and T. Duke. Conformational spread: The propaga

[62] R. Endres, O. Oleksiuk, C. Hansen, Y. Meir, V. Sourjik, and N. Wingreen. Variable sizes of Escherichia coli chemoreceptor signaling teams.

[88] E. Keller and L. Segel. Model for chemotaxis. Journal of Theoretical Biology, 30(2):225{234, 1971.

[89] D. Horstmann. From 1970 until present: The Keller-Segel model in chemotaxis and its consequences I.

[100] R. Erban and H. Othmer. From individual to collective behavior in bacterial chemotaxis. SIAM Journal on Applied Mathematics, 65(2):361{391, 2004.

[101] C. Patlak. Random walk with persistence and external bias. The Bulletin of Mathematical Biophysics

[114] R. Stewart, K. Jahreis, and J. Parkinson. Rapid phosphotransfer to CheY from a CheA protein lacking the CheY-binding domain. Biochemistry, 39(43):13157{13165, 2000.

[115] R. Stewart, A. Roth, and F. Dahlquist. Mutations that a ect control of the methylesterase activity of CheB, a component of the chemotaxis adaptation system in Escherichia coli. Journal of Bacteriology, 172(6):3388{3399, 1990.

[116] J. Smith, J. Latiolais, G. Guanga, S. Citineni, R. Silversmith, and R. Bourret. Investigation of the role of electrostatic charge in activation of the Escherichia coli response regulator CheY. Journal of Bacteriology, 185(21):6385{6391, 2003.

[117] D. Bray. Research group data. http://www.pdn.cam.ac.uk/groups/comp-cell/Data.html. Accessed: 08/05/2012.

[118] T. Shimizu, Y. Tu, and H. Berg. A modular gradient-sensing network for chemotaxis in Escherichia coli revealed by responses to time-varying stimuli. Molecular Systems Biology, 6(1), 2010.

[119] A. Vaknin and H. Berg. Physical responses of bacterial chemoreceptors. Journal of Molecular Biology, 366(5):1416{1423, 2007.

[120] P. Dunten and D. Koshland. Tuning the responsiveness of a sensory receptor via covalent modi cation. Journal of Biological Chemistry

[138] S. Kalir, J. McClure, K. Pabbaraju, C. Southward, M. Ro